Sleep Research Society®

Article Navigation

EDITOR'S
CHOICE

Melanin-concentrating hormone-expressing neurons adjust slow-wave sleep dynamics to catalyze paradoxical (REM) sleep FREE

Christophe Varin, Pierre-Hervé Luppi, Patrice Fort

Sleep, Volume 41, Issue 6, June 2018, zsy068, https://doi.org/10.1093/sleep/zsy068
Published: 29 March 2018 **Article history ▾**

PDF Split View Cite Permissions Share ▾

Abstract

Study Objectives

Experimental studies over the last 15 years established a role in sleep of the tuberal hypothalamic neurons that express melanin-concentrating hormone (MCH). Controversies still remain regarding their actual contribution to both slow-wave sleep (SWS) and paradoxical sleep (PS also known as REM sleep) or PS alone.

Methods

To address this point, we compared effects of chemogenetic activation and inhibition of MCH neurons on SWS and PS amounts and EEG rhythmic activities in transgenic *Pmch-cre* mice.

Results

In agreement with recently reported optogenetic data, the activation of MCH neurons invariably facilitates PS onset and maintenance. Our chemogenetic experiments further disclose that the ultradian rhythm of SWS is also notably related to the activity of MCH neurons. We observed that the mean duration of SWS episodes is significantly extended when MCH neurons are inhibited. Conversely, when they were excited, SWS bouts were drastically shortened and depicted substantial changes in δ rhythmic activities in electroencephalographic recording likely reflecting a deeper SWS.

Conclusions

According to these original findings, we propose that when MCH neurons are physiologically recruited, SWS depth is increased and the extinction of SWS episodes is accelerated, two joint physiological processes strengthening the probability for natural SWS to PS transition and likely facilitating PS onset.

melanin-concentrating hormone, tuberal hypothalamus, DREADD, pharmacogenetics, CNO, REM sleep, slow-wave sleep

Statement of Significance

Multiple studies identified hypothalamic neurons expressing melanin-concentrating hormone (MCH) as a major system involved in paradoxical sleep regulation. However, their precise contribution in the control of slow-wave sleep remains elusive. Using pharmacogenetic manipulation of their activity, we demonstrated that MCH neurons actually participate in slow-wave sleep control by facilitating the occurrence of a deeper slow-wave sleep state and by accelerating the termination of slow-wave sleep episodes. These results provide new insights into the function of MCH neurons and their potent involvement in other physiological processes associated with sleep.

Introduction

Neurons that express melanin-concentrating hormone (MCH) constitute a molecularly defined neuronal subpopulation distributed within the tuberal hypothalamus and zona incerta [1]. Several results point to a pivotal implication of MCH-expressing neurons in the control of sleep, in particular paradoxical (or REM) sleep (PS) [2–4]. Indeed, these neurons strongly express the immediate early gene c-Fos after PS rebound following short or long-lasting PS deprivations in rats [5–8] and mice [9]. Accordingly, MCH neurons discharge maximally during PS episodes as measured using juxtacellular recordings across natural sleep-waking cycle in head-restraint rats [10]. Furthermore, optogenetic stimulation of MCH neurons facilitates PS onset and maintenance [11–15], suggesting their downstream control of brainstem PS-generating networks [2, 4, 16]. Regarding slow-wave sleep (SWS), puzzling results were reported in these optogenetic studies, likely due to the use of dissimilar illumination protocols. Indeed, chronic stimulation of MCH neurons increased SWS amounts only during the dark phase [12, 14], whereas the continuous stimulation for 3 hours during the light phase decreased SWS amounts [13]. Moreover, acute illumination of MCH neurons when applied just at the onset of a SWS episode did not change the duration of the ongoing episode [11]. In addition, cell-specific ablation of MCH neurons failed to demonstrate any prominent effect on PS [13, 15, 17], whereas SWS amounts were decreased due to shortened SWS bouts [13, 17]. Finally, chemogenetic activation of MCH neurons caused specific increases in PS without affecting SWS [15].

Despite obvious experimental efforts in recent years [18], the precise contribution of MCH-expressing neurons to SWS and/or PS regulation remains elusive. In an attempt to bridge this gap, we examined effects of their chemogenetic activation and inhibition on PS, SWS, and electroencephalographic (EEG) rhythmic activities across the vigilance states in behaving mice. This approach relies on the genetically targeted expression of either inhibitory hM4di– or excitatory hM3dq–mutated muscarinic receptors activated by their specific ligand clozapine-N-oxide (CNO) [19, 20].

Using pharmacogenetics, we were able to show that MCH neurons play a significant role, in addition to PS consolidation, in SWS expression by simultaneously potentiating the termination of SWS episodes and favoring deep sleep. Both modulatory mechanisms may strengthen the probability for the natural SWS to PS transition that may concur for promoting PS.

Materials and Methods

All experiments were carried out in application of the 3R principles in animal experiments, in strict accordance with the European Union directive 2010/63/EU and recommendations in the guide for the Care and Use of laboratory Animal of the National Institutes of Health (NIH publication no. 85-23). Protocols and procedures were approved by the local *Comité d'Éthique en Expérimentation Animale* of Lyon I University (C2EA-55) and the French *Ministère de l'Enseignement Supérieur, de la Recherche et de l'Innovation* (DR2014-39).

Animals

The mouse strain used, STOCK Tg(Pmch-cre)KY133Gsat/Mmucd (identification number 034699-UCD), was obtained from the Mutant Mouse Regional Resource Center, a NCRR-NIH funded strain repository, and was donated to the MMRRC by the NINDS funded GENSAT BAC transgenic project. Heterozygous Tg(*Pmch-cre*) mice were maintained under a C57BL/6 genetic background. Mice were bred in a temperature-controlled room (22 ± 1°C) exposed to a standard 12/12 hr light-dark cycle (light on at 8 am). Founders and subsequent offspring were genotyped by PCR amplification of genomic DNA using the following primer sets (Eurofins Scientific, France): forward, GAT CTC CGG TAT TGA AAC TCC AGC; reverse, GCT AAA CAT GCT TCA TCG. Once genotyped, mice were weaned at 3–4 weeks of age, grouped, and housed according to gender with ad libitum access to food and water.

Surgical preparation of animals

Male Tg(*Pmch-cre*) mice (8–10 weeks old) were anesthetized by an intraperitoneal (i.p.) injection with a mixture of ketamine and xylazine (100 and 10 mg/kg; Ceva Santé Animale, France) and placed on a stereotaxic frame (David Kopf Instruments, USA). Viral vectors (AAV_{10}-hSyn-DIO-hM3dq-mCherry, AAV_{10}-hSyn-DIO-hM4di-mCherry or AAV_{10}-hSyn-DIO-mCherry; a donation from M. Lazarus [21]) were bilaterally infused (800 nL at 50 nL/min) under stereotaxic control in the tuberal hypothalamus (AP: −1.50 mm; ML; ±0.95 mm; DV: −5.35 mm relative to Bregma, Paxinos and Franklins, 2012) through a cannula connected to a Hamilton syringe (10 μL) placed in a syringe pump (UMP3; World Precision Instruments, USA). Cannula was lowered into the brain and left in place for 5 min before and 10 min after infusion. After AAV administration, all mice were prepared for polysomnographic recordings as described previously [9, 17]. Briefly, two stainless steel screws were inserted into the skull above the right parietal (1.7 mm lateral to midline and 2.5 mm posterior to Bregma) and frontal (1.1 mm lateral and 1.5 mm anterior) cortices; a third reference electrode was fixed above the cerebellum (1 mm lateral and 5 mm posterior). Two wire electrodes ending by a gold-coated tin drop (about 1 mm diameter, AlphaWire, UK) were inserted in between neck muscles for a differential electromyographic (EMG) recording. All electrodes were connected into a miniature pedestal (Plastics One, Bilaney, Germany) and fixed to the skull with Super-Bond (C&B, Sun Medical Co. Ltd, Japan) and dental cement (Paladur, Heraeus Kuzler, Germany). At the end of surgery, Carprofen (5 mg/kg) was subcutaneously administered for pain caring. Hereafter, mice were housed in individual Plexiglas barrels (diameter 25 cm; height 40 cm) with woodchip bedding and ad libitum access to food (Extra Labo, France).

Sleep recordings and CNO administration

After 7 days of postsurgical recovery, mice were transferred to an insulated soundproof box maintained under the standard laboratory conditions (12/12 hr light-dark cycle, lights on at 8 am, 22 ± 1°C). Mice were connected to a cable plugged to a rotating connector (Plastics One, Bilaney, Germany) to allow free movements. After 3 days of habituation, mice were continuously recorded and received pharmacological i.p. clozapine N-oxide (CNO; C0832, Sigma-Aldrich) dissolved in 0.9% saline (Vehicle) in volumes of 5 mL/kg in randomized order spaced by at least 48 hr. Five doses of CNO were used as follows: 0.2, 0.5, 1, 5, and 10 mg/kg. Precisely, control mice (AAV_{10}-DIO-mCherry; $n = 10$) were treated with Vehicle (NaCl), and CNO at 0.5, 1, 5, and 10 mg/kg; hM3dq-expressing mice were injected with Vehicle, 0.5, and 1 mg/kg CNO at 8 am ($n = 10$) or Vehicle, 0.2, 0.5, and 1 mg/kg CNO at 8 pm ($n = 10$); and hM4di-transfected mice received Vehicle, 1, and 5 mg/kg CNO administrations at 8 am ($n = 9$), and Vehicle, 1, and 5 mg/kg CNO injections at 8 pm ($n = 6$). No effect of the order in which CNO doses were administered was observed. Before the pharmacological process, mice were daily handled during 10 min and habituated to injections during at least 7 days. Unipolar EEG and bipolar EMG signals were amplified (MCP+, Alpha-Omega Engineering, Israel), analog-to-digital converted with a sampling rate of 520.8 Hz, and collected on a computer via a CED-1401 Plus interface with Spike2 software (Cambridge Electronic design, CED, UK).

Data analysis

Animals' behavioral states were scored by 5 s epochs and classified as waking, SWS, and PS based on the visual inspection of EEG/EMG signals. During waking, activated low-amplitude EEG is accompanied by a sustained EMG activity with phasic bursts. SWS is characterized by high-voltage EEG slow waves, spindles, and the disappearance of phasic muscle activity. PS is characterized by a decrease in the EEG amplitude associated with a flat EMG (muscle atonia) and a regular and pronounced θ rhythm. Hypnograms were then drawn using a custom script in Spike2 (CED, UK). Standard parameters for each vigilance state (amounts, numbers of bouts, mean durations of episodes, and latencies) were computed over the first 3 hr following each treatment. Additionally the probability of SWS to PS transition was estimated by computing the ratio of the number of PS episodes to the number of SWS episodes.

Spectral analysis of EEG signals was performed using a fast Fourier transform (0.1 Hz resolution) on 5 s artifact-free epochs over the first 3 hr following treatments. Spectra were subsequently normalized by the power over the entire frequency range (0.5–45 Hz) computed from recordings collected during the first 3 hr following Vehicle injections. This normalization factor was then applied to signals recorded after CNO treatments. The mean spectral power was calculated by averaging spectra for each vigilance state for each animal.

Spindle detection and analysis

For the detection of sleep spindles during SWS, frontal EEG recordings were band-pass filtered between 7 and 15 Hz. The root mean square (rms) of the filtered signal was computed on sliding windows of 1 s duration at 0.25 s intervals [22, 23]. SWS epochs were considered containing spindles when the rms value exceeded the 95th percentile of the computed rms distribution. To take into account the waning and waxing property of spindles, a maximal interruption period of one 0.25 s interval within an individual spindle was allowed. Detected spindles longer than 5 s or shorter than 0.5 s were discarded. Spindle density during SWS was defined as the number of spindles whose center occurs during SWS and was quantified per 1 min of SWS. The proportion of SWS time containing spindles was defined as the amount of SWS containing spindles and expressed as a percentage of SWS

amounts.

Ex vivo electrophysiology

For electrophysiological ex vivo recordings, slices were obtained from 8–12 weeks old Tg(*Pmch-cre*) mice (males and females) that received viral vector injections in the tuberal hypothalamus at least 3 weeks before use. All experiments were performed during the light period. Animals were deeply anesthetized (sodium pentobarbital, 150 mg/kg, i.p., Ceva Santé Animale, France) and transcardially perfused with ice-cold sucrose ACSF that contained the following (in mM): 2.5 KCl, 0.5 $CaCl_2$, 25 $NaHCO_3$, 1.2 NaH_2PO_4, 10 $MgSO_4$, 25 D-glucose, and 185 sucrose (pH 7.35). After decapitation, brains were quickly removed. Coronal hypothalamic slices (300 µm-thick) were cut with a vibrating microtome in the same ice-cold ACSF. They were subsequently transferred in warm (~33°C) ACSF containing (in mM): 130 NaCl, 5 KCl, 2.4 $CaCl_2$, 20 $NaHCO_3$, 1.25 KH_2PO_4, 1.3 $MgSO_4$, 10 D-glucose, 15 sucrose, and 1 kynurenate (pH 7.35) and constantly oxygenated (95% O_2/5% CO_2). They were left to recover for at least 30 min. Individual slices were then transferred to a thermoregulated (32.5 °C) chamber (Badcontroller V; Luigs & Neumann, Germany), placed under a microscope (Axioscop2; Zeiss, Germany) equipped with an infrared CCD camera (Hamamatsu, Japan). Slices were maintained immersed at room temperature and continuously surperfused at 3–5 mL/min with oxygenated kynurenate-free ACSF. All electrophysiological experiments were performed with an Axopatch 200B (Molecular Devices, USA) amplifier connected to an acquisition board (Digidata 1200B; Molecular Devices) attached to a computer running pCLAMP software (Molecular Devices). Whole-cell patch-clamp recordings were performed with patch-clamp pipettes (3–6 MΩ) filled with 8 µL of internal solution containing (in mM): 144 K-gluconate, 3 $MgCl_2$, 0.2 EGTA, 10 HEPES (pH 7.2, 285–295 mOsm). The pipette was slowly brought to on the selected neuron to be recorded in whole-cell configuration using infrared videomicroscopy guidance and clamped at −60 mV. During whole-cell patch-clamp recordings, the intrinsic membrane properties of neurons were assessed by applying current steps (800 ms) from −100 pA to firing saturation in 10 pA increments. Clozapine N-oxide (CNO; C0832, Sigma-Aldrich) was freshly dissolved before each recording session in ACSF at 10 µM from stock solutions of CNO (10 mM; DMSO) that were stored as frozen aliquots at −20°C.

Immunohistochemistry

At the end of polysomnographic recordings, all the mice were perfused to control the location of AAV_{10} injection sites as well as the specificity and efficiency of transfection in MCH neurons. Animals with unilateral injection or insufficient AAV spreading over the tuberal hypothalamus and transfection efficiency of MCH neurons (below 50%) were discarded from subsequent sleep analysis. Additionally, a subset of Tg(*Pmch-cre*) mice that were transfected with AAV_{10}-hSyn-DIO-hM3dq-mCherry received a last CNO (1 mg/kg) or Vehicle injection (n = 3 per condition) at 8 am and was perfused 120 min later to evaluate c-Fos expression in hM3dq-expressing MCH neurons. Briefly, mice were deeply anesthetized (sodium pentobarbital, 150 mg/kg, i.p., Ceva Santé Animale, France) and then transcardially perfused with Ringer's lactate solution containing 0.1% heparin followed by 50 mL of an ice-cold fixative composed of 4% paraformaldehyde in 0.1 M phosphate buffer (PB, pH 7.4). Brains were postfixed for 24 hr at 4°C in the same fixative, dipped in PB containing 30% sucrose for 2 days, and finally frozen in methyl-butane cooled with dry ice. Using a cryostat, brains were then cut serially in coronal sections (30 µm thick). Free-floating sections were collected in PBS with 0.03% Triton X100 (PBST) and stored until use in the same buffer containing 0.1% sodium azide (PBST-Az).

The dual immunodetection of MCH and mCherry was performed by incubation of hypothalamic sections in rabbit anti-MCH (1:20,000; Abcam, UK) and rat anti-mCherry (1:50,000; Invitrogen, USA) antibodies in PBST-Az for 3 days at 4°C. After three rinses in PBST, revelation was performed using donkey anti-rabbit Alexa 488 and goat anti-rat Alexa 568 (1:500 each; Invitrogen) fluorescent secondary antibodies in PBST at room temperature during 120 min. Immunodetection of orexin neurons was performed as described above using goat anti- orexin-A (1:2,000; PBST-Az; Santa Cruz, USA) and donkey anti-goat Alexa 488 (1:500; PBST; Invitrogen) as primary and secondary antibodies, respectively. The sections were finally mounted on glass gelatin-coated slides and coverslipped with Fluoromount (SouthernBiotech, USA).

The dual immunodetection of MCH and c-Fos was obtained by sequential incubations of the free-floating sections in (1) a rabbit anti-c-Fos antiserum (1:8,000; Merck, USA) in PBST-Az for 3 days at 4°C, (2) a biotinylated goat anti-rabbit IgG (1:1,000; Vector Laboratories, UK) for 90 min at room temperature, and (3) an ABC-HRP complex (1:1,000; Elite kit; Vector Labs) for 90 min at room temperature. The sections were then immersed in (4) 0.05 M Tris-HCl buffer, pH 7.6, containing 0.025% 3,3'-diaminobenzidine tetrahydrochloride (DAB; Sigma-Aldrich, France), 0.003% H_2O_2, and 0.6% nickel ammonium sulfate for 20 min at room temperature. Three 10 min washes were performed between each incubation step. The staining appeared as a dense black nuclear coloration of c-Fos-immunoreactive neurons. After extensive rinses, pretreated sections were incubated with (5) rabbit anti-MCH (1:50,000, Phoenix Pharmaceuticals, USA) for 72 hr at 4°C, (6) biotinylated anti-rabbit IgG (1:1,000 in PBST; Vector Labs) for 90 min at room temperature, (7) an ABC-HRP complex (1:1,000 in PBST) for 90 min at room temperature, and (8) 0.05 M Tris-HCl buffer containing 0.025% 3,3'-diaminobenzidine-4 HCl and 0.003% H_2O_2 for 20 min. The cytoplasm and primary dendrites of MCH neurons were colored in orange-

brown.

Counting procedure was conducted for each mouse as follows: four labeled sections evenly spaced every 270 μm throughout the extent of the lateral hypothalamus (from AP −1.2 mm to AP −2.4 mm relative to Bregma) were analyzed with an Axioskop 2 microscope (Zeiss, Germany) equipped with a motorized X–Y-sensitive stage and a video camera connected to a computerized image analysis system (ExploraNova, France). Labeled neurons were bilaterally plotted and automatically counted using Mercator v.2 software (ExploraNova). Photomicrographs were taken with a CCD Color 10-bit QiCam camera, imported into Adobe Photoshop 10, digitally adjusted for brightness and contrast, and were assembled into plates at a resolution of 300 dpi. Histological data are reported for all the mice with MCH neuron transfection efficiency above exclusion criterion and used for polysomnographic recordings.

Statistics

Statistical significance was set at 0.05 for all procedures detailed below. The effects of CNO bath-application on neuronal activity recorded ex vivo were tested with nonparametric Friedman tests (baseline vs. CNO application vs. washout) followed by post hoc Wilcoxon tests to detect pairwise differences. Differences in c-Fos straining in MCH neurons after Vehicle or CNO treatments were evaluated using nonparametric Mann–Whitney tests. Regarding polysomnographic recordings, sleep parameters obtained after CNO treatments at 8 am were compared using permutation-based mixed-design ANOVA (two-ways with one-factor replication) followed by permutation-based post hoc tests to compare within each group paired differences between CNO vs. Vehicle treatments and permutation-based post hoc tests to compare the effects of CNO treatments vs. Vehicle between the different groups of mice. Parameters extracted from spectral analyses (power over a given frequency band, frequency of the peak in power over the θ band) were compared across genotypes and across CNO treatments following the same procedure. Sleep parameters computed from injections performed at 8 pm in hM3dq or hM4di mice were compared using permutation-based rmANOVA (with one-factor replication) followed by permutation-based post hoc tests to compare within each group paired differences between CNO vs. Vehicle treatments.

Results

hM3dq or hM4di receptors are functional when genetically expressed in MCH neurons

To manipulate the activity of MCH neurons, we bilaterally infused adeno-associated virus vectors (AAV) encoding either excitatory hM3dq or inhibitory hM4di receptors fused to the fluorescent mCherry reporter into the tuberal hypothalamus and zona incerta of Tg(*Pmch-cre*) mice. Firstly, the selectivity of the genetic targeting was assessed by the immunodetection of MCH (in green) and mCherry (in red) in hypothalamic sections from these mice (Figure 1A and B). Immunostaining for mCherry was detected in 68.3 ± 3.3% (n = 10 mice) and 62.1 ± 2.1% (n = 9 mice) of MCH-immunoreactive neurons in the hM3dq- and hM4di-transfected mice used for polysomnographic recording, respectively. In detail, mCherry expression was found in 71.5 ± 3.3% and 66.4 ± 4.3% of MCH neurons within the zona incerta, 70.0 ± 3.3% and 61.2 ± 1.5% within the lateral part of tuberal hypothalamus, and in 62.3 ± 3.3% and 60.6 ± 1.8% within the medial tuberal hypothalamus, respectively, in hM3dq- and hM4di-expressing mice. In our sample (n = 19 mice), we observed that the above areas account for 17.8 ± 1.0% (zona incerta), 57.1 ± 0.9% (lateral tuberal hypothalamus), and 25.1 ± 0.6% (medial tuberal hypothalamus) of the total MCH population. MCH immunolabeling was observed in 97.2 ± 0.2% and 97.6 ± 0.2% of mCherry-immunoreactive neurons, respectively. No mCherry labeling was seen in neighboring orexin-immunoreactive neurons (Figure 1C). Secondly, whole-cell recordings of mCherry-expressing neurons in acute hypothalamic slices revealed depolarization in hM3dq-expressing neurons (+13.8 ± 0.7 mV; n = 4; Wilcoxon test, $p < 0.05$) and hyperpolarization in hM4di-expressing cells (−8.4 ± 1.2 mV; n = 4; Wilcoxon test, $p < 0.05$) upon bath application of clozapine N-oxide (CNO, 10 μM) (Figure 1D), thus demonstrating the functional efficacy of chemogenetic receptors when expressed in MCH neurons. Finally, CNO administration (1 mg/kg; i.p.) in hM3dq-transfected mice 2 hr prior to sacrifice resulted in an enhanced expression of c-Fos, a marker of neuronal activation, in MCH-immunoreactive neurons compared with hM3dq-transfected mice injected with Vehicle (Vehicle: 0.9 ± 0.2%; CNO: 31.5 ± 2.6%; n = 3 mice per condition; Mann–Whitney test, p = 0.05; Figure 1E). Taken together, these results ascertain the specificity of our molecular targeting method and efficiency of chemogenetics as reliable tools to bidirectionally control the activity of MCH neurons.

Figure 1.

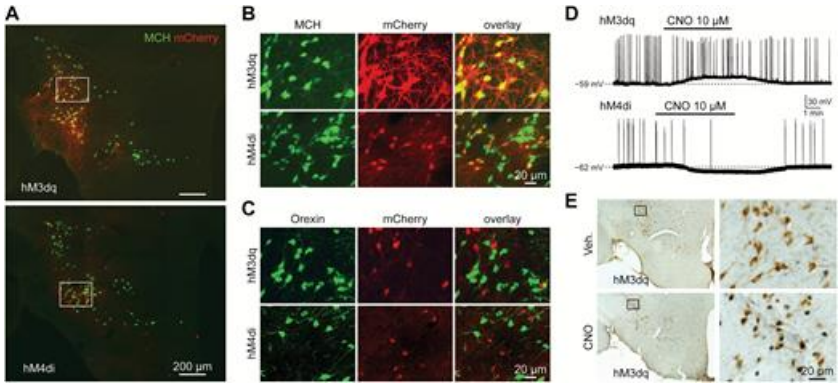

View large Download slide

Chemogenetic receptors are functional when expressed in MCH neurons. **(A)** Photomicrographs of frontal hypothalamic sections from Tg(*Pmch-cre*) mice expressing hM3dq (top) or hM4di (bottom) chemogenetics double immunostained for MCH (green) and reporter protein mCherry (red). Note the high number of double-labeled (yellow) cell bodies. **(B)** Higher magnification photomicrographs of the same sections (boxes in A). **(C)** High magnification photomicrographs of adjacent sections from the same transducted mice depicting mCherry fluorescent neurons (red) and cell bodies immunolabeled for orexin (green). No co-expression of fluorescent markers was encountered. **(D)** Effects of bath-applied CNO (10 µM) on the membrane potential of representative hM3dq- (upper panel) or hM4di-expressing (lower panel) neurons recorded in whole-cell configuration from acute brain slices. **(E)** Coronal hypothalamic sections from two representative hM3dq mice injected with Vehicle (upper panels) or CNO (1 mg/kg; lower panels) 2 hr prior perfusion. These sections were then double immunostained for c-Fos (nuclei colored in black) and MCH (brown colored cytoplasms). As evidenced at high magnification (boxes), numerous MCH-immnolabeled neurons express early gene c-Fos only after CNO treatment, indicating that they have been activated by CNO treatment.

Evidence for CNO side effects on vigilance states

Upon systemic administration, CNO can be rapidly reduced into clozapine, an atypical antipsychotic with potent effects on sleep [24–26]. In our hands, CNO indeed dose-dependently increased SWS and decreased PS amounts in Tg(*Pmch-cre*) littermates transfected with control AAV only encoding for the fluorescent mCherry reporter (Ctrl mice; Supplementary Figure S1, A–C). Significant effects were observed for CNO doses above 5 mg/kg and reflected decreased numbers of both PS and SWS episodes, increased duration of SWS episodes, and delayed latencies to the first PS episode after CNO treatments (Supplementary Figure S1, D–F). These CNO-induced side effects must be taken into account and properly controlled to discriminate those specifically due to the activation of hM3dq or hM4di receptors. In this study, we decided therefore to investigate CNO effects on the sleep-waking cycle by using a large range of CNO doses (vs. Vehicle) in hM3dq- and hM4di-transfected mice. To overcome these side effects, data in hM3dq or hM4di mice were also directly compared with those in Ctrl littermates treated at the same CNO doses (Figure 2).

Figure 2.

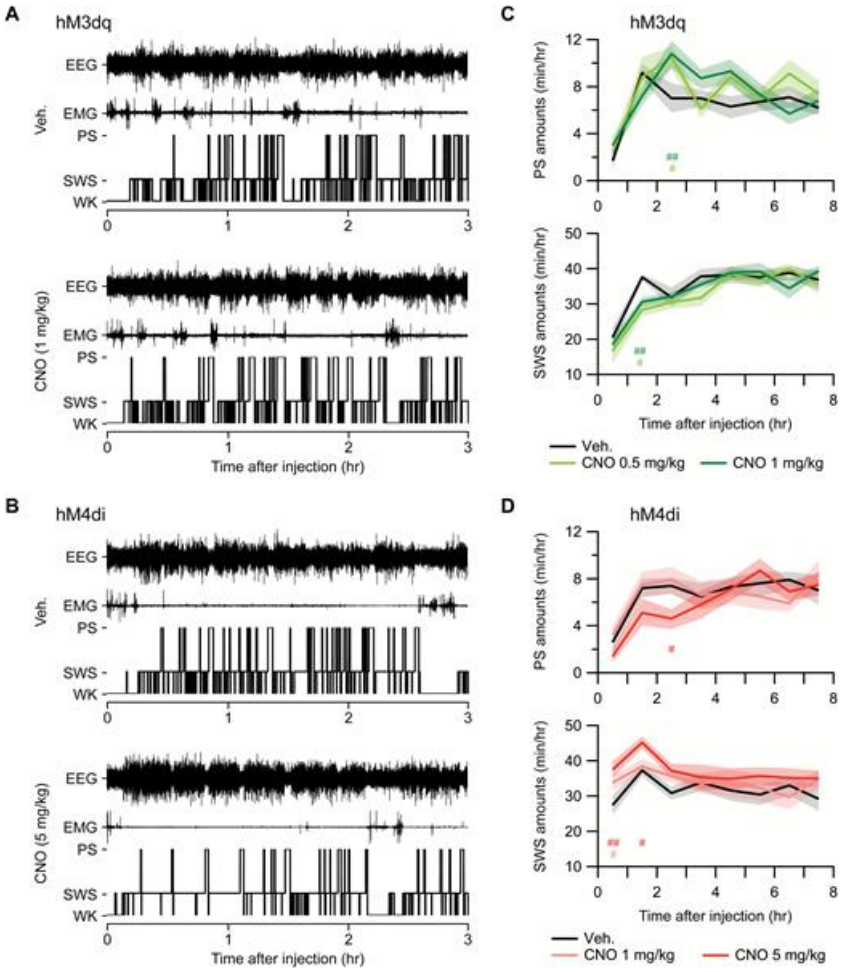

View large Download slide

Chemogenetic excitation and inhibition of MCH neurons impact sleep. **(A)** and **(B)** Examples of EEG/EMG polysomnographic recordings and corresponding hypnograms obtained from one representative hM3dq (A) and hM4di (B) mice during the first 3 hr (8–11 am) following Vehicle (top) and CNO (bottom) administrations. **(C)** and **(D)** Hourly distribution of PS (top) and SWS (bottom) amounts (min/hr) over the first 8 hr (8 am–4 pm) following Vehicle and CNO injections at two different doses in hM3dq mice (C; 0.5 and 1 mg/kg; $n = 10$) and in hM4di mice (D; 1 and 5 mg/kg; $n = 9$) (permutation-based two-way rmANOVA: for all measurements interaction time × CNO doses, $p < 0.05$; post hoc test vs. Vehicle: $^{\#}p < 0.05$; $^{\#\#}p < 0.01$). Data for Vehicle and individual doses of CNO tested are represented as mean (lines) ± SEM (light colors). See also Supplementary Figure S1.

MCH neurons regulate PS promotion and maintenance

Here, we found that the CNO-induced activation of MCH neurons at light onset (8 am) in hM3dq (vs. Ctrl) mice specifically increased PS amounts during the first 3 hr following CNO injections at a dose of 0.5 mg/kg (Figures 2A, C, and 3A). Conversely, the inhibition of MCH neurons in hM4di mice did not affect PS amounts compared with respective Ctrl mice (Figures 2B, D, and 3A). We next quantified two parameters directly related to PS promotion, i.e. the number of PS episodes and the latency to the first PS episode after CNO or Vehicle injections. In both hM3dq and hM4di mice, the number of PS episodes was not significantly affected by CNO treatments when compared with Ctrl animals (Supplementary Figure S2A). However, chemogenetic activation of MCH neurons significantly decreased the latency to the first PS episode, whereas no effect was observed in hM4di mice (Figure 3B), supporting a facilitating role of MCH neurons in PS onset. Then, the analysis of mean PS episodes duration following CNO treatments revealed that the excitation of MCH neurons significantly extended the mean duration of PS episodes compared with respective Ctrl animals, whereas their inactivation had no prominent effect (Figure 3B). Regarding EEG oscillatory activities during PS, we found that chemogenetic activation of MCH neurons induced modifications in θ rhythm (Figure 3C and D) by significantly increasing its peak frequency (Figure 3E) and total spectral power within the whole θ frequency range (Figure 3F). No such changes were noticed upon the chemogenetic inhibition of MCH neurons (Supplementary Figure S2, B–E).

Figure 3.

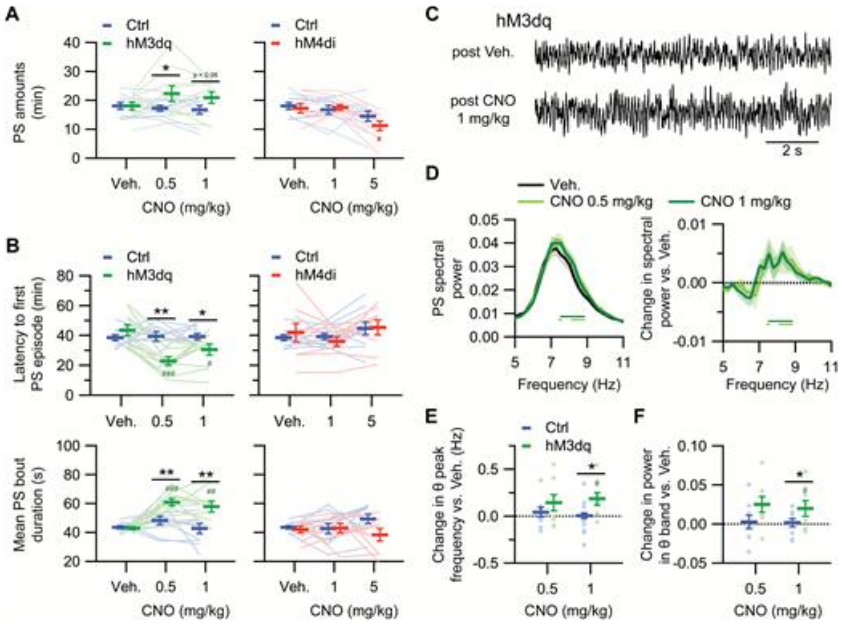

View large Download slide

MCH neurons contribute to PS promotion and maintenance. **(A)** PS amounts during the first 3 hr (8–11 am) following Vehicle and CNO treatments in hM3dq mice (n = 10; green; left panel) (permutation-based mixed-design ANOVA: CNO doses, p = 0.19; Ctrl/hM3dq, p = 0.15; interaction, $p < 0.05$; post hoc test vs. Vehicle: $^{\#}p < 0.05$; post hoc test vs. Ctrl mice: $^{*}p < 0.05$), and in hM4di mice (n = 9; red; right panel) (permutation-based mixed-design ANOVA: CNO doses, $p < 0.01$; Ctrl/hM4di, p = 0.84; interaction, p = 0.12; post hoc test vs. Vehicle: $^{\#}p < 0.05$) compared with respective Ctrl mice (n = 10; blue). **(B)** Latency to the first PS episodes (top panels) and mean duration of PS episodes (bottom panels) during the first 3 hr following Vehicle and CNO treatments in hM3dq mice (n = 10; green; right panels) compared with Ctrl mice (n = 10; blue) (permutation-based mixed-design ANOVA: for PS latency: CNO doses, $p < 0.001$; Ctrl/hM3dq, $p < 0.05$; interaction, $p < 0.001$; for mean duration: CNO doses, $p < 0.001$; Ctrl/hM3dq, $p < 0.05$; interaction, $p < 0.05$; post hoc test vs. Vehicle: $^{\#\#}p < 0.01$, $^{\#\#\#}p < 0.001$; post hoc test *vs.* Ctrl mice: $^{*}p < 0.05$; $^{**}p < 0.01$) and in hM4di (n = 9; red; right panels) mice compared with the same Ctrl mice (n = 10; blue) (permutation-based mixed-design ANOVA: for PS latency: CNO doses, p = 0.11; Ctrl/hM4di, p = 0.99; interaction, p = 0.48; for mean duration: CNO doses, p = 0.95; Ctrl/hM4di, p = 0.16; interaction, p = 0.11). In graphs A–B, individual data for each mouse are displayed (lines; light colors) and averaged data are represented as mean ± SEM (bars). **(C)** Examples of parietal EEG signals recorded during PS after CNO or Vehicle treatments in a representative hM3dq mouse. **(D)** Spectral power (left panel) and changes in spectral power compared with Vehicle treatment (right panel) obtained from parietal EEG recordings and calculated from PS bouts during the first 3 hr following CNO or Vehicle injections in hM3dq mice (n = 8) (permutation-based two-way rmANOVA; CNO doses, $p < 0.05$, frequency, $p < 0.001$, interaction, $p < 0.05$; post hoc test vs. Vehicle, horizontal bars below spectra indicate $p < 0.05$). Spectral data for individual doses of CNO tested are represented as mean (lines) ± SEM (light colors). **(E)** and **(F)** Change in θ peak frequency (E) and in power over the θ band (F) relative to Vehicle during PS episodes following CNO injections in hM3dq mice (n = 8; green) and Ctrl mice (n = 9; blue) (permutation-based mixed-design ANOVA: for θ peak frequency: CNO doses, $p < 0.05$; Ctrl/hM3dq, p = 0.11; interaction, $p < 0.01$; for θ power: CNO doses, $p < 0.01$; Ctrl/hM3dq, $p < 0.05$; interaction, $p < 0.05$; post hoc test vs. Vehicle: $^{\#}p < 0.05$; post hoc test vs. Ctrl mice: $^{*}p < 0.05$). Individual data for each mouse are displayed (dots; light colors) and averaged data are represented as mean ± SEM (bars). See also Supplementary Figure S2.

The same samples of hM3dq and hM4di mice also received CNO injections at the onset of the active period (8 pm). In hM3dq mice, CNO (0.2 and 0.5 mg/kg) increased PS amounts, number of PS episodes, and their mean duration (Supplementary Figure S2, F–H) and decreased latencies to the first PS episode (Supplementary Figure S2I). These PS-facilitating effects were not maintained at higher doses (1 mg/kg) putatively reflecting a saturation of action potentials generation when hM3dq receptors are too strongly activated. No significant effect was found in hM4di mice regarding any of PS-related parameters analyzed (Supplementary Figure S2, J–K).

In conclusion, our chemogenetic experiments replicate recent optogenetic data highlighting that MCH neurons, when activated, contribute to PS promotion and consolidation.

MCH neurons contribute to SWS termination and adjust EEG rhythms during SWS

Since natural PS physiologically emerges from SWS, we then compared SWS properties after CNO injections in hM3dq and hM4di mice with Ctrl ones. During the first 3 hr post-treatment at light onset (8 am), SWS amounts were significantly decreased in hM3dq vs. Ctrl mice. Conversely,

hM4di mice showed increased SWS amounts (Figures 2 and 4A). These consistent data suggest that MCH neurons, when active, impede SWS. We next extended analysis to outline processes underpinning this inhibitory role. We found that the duration of SWS episodes was reciprocally modulated by CNO treatments in hM3dq and hM4di mice. Indeed, the activation of MCH neurons shortened mean SWS episode duration (Figure 4B and C). Conversely, after the inhibition of MCH neurons, the mean duration of SWS episodes was significantly extended (Figure 4B), and the proportion of longer SWS episodes was increased (Figure 4C). Concomitantly, the number of SWS episodes and latency to the first SWS episode was not significantly modified in CNO-treated hM3dq or hM4di mice (Supplementary Figure S3, A and B). Taken together, the above results indicate that the impeding role of MCH neurons may not rely on alterations of SWS promotion but should rather implicate mechanisms of SWS consolidation.

Figure 4.

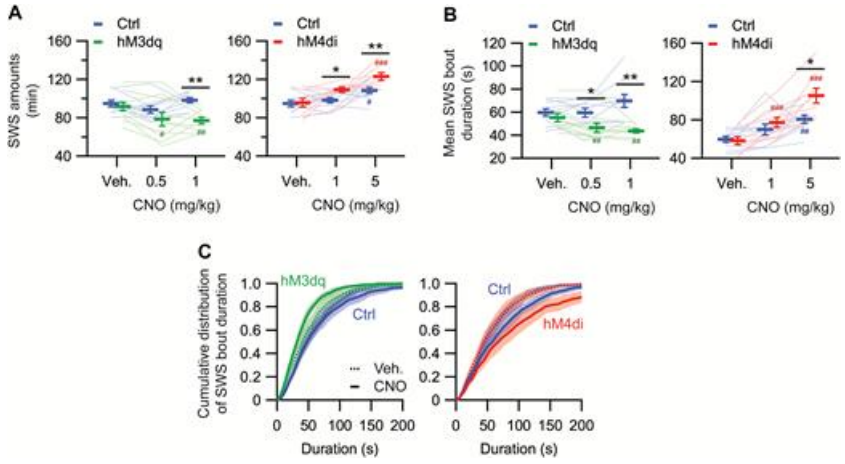

View large Download slide

MCH neurons control the duration of SWS episodes. **(A)** SWS amounts during the first 3 hr (8–11 am) following CNO treatments in hM3dq mice (n = 10; green; left panel) compared with Ctrl mice (n = 10; blue) (permutation-based mixed-design ANOVA: CNO doses, $p < 0.01$; Ctrl/hM3dq, $p < 0.05$; interaction, $p < 0.05$; post hoc test vs. Vehicle: $^{\#}p < 0.05$, $^{\#\#}p < 0.01$; post hoc test vs. Ctrl mice: $^{*}p < 0.05$, $^{**}p < 0.01$) and in hM4di mice (n = 9; red; right panels) compared with Ctrl mice (permutation-based mixed-design ANOVA: CNO doses, $p < 0.001$; Ctrl/hM3dq, $p < 0.05$; interaction, $p < 0.05$; post hoc test vs. Vehicle: $^{\#}p < 0.05$, $^{\#\#\#}p < 0.001$; post hoc test vs. Ctrl mice: $^{*}p < 0.05$, $^{**}p < 0.01$). **(B)** Mean SWS bout duration following CNO treatments in hM3dq mice (n = 10; green; left panels) (permutation-based mixed-design ANOVA: CNO doses, $p = 0.12$; Ctrl/hM3dq, $p < 0.01$; interaction, $p < 0.05$; post hoc test vs. Vehicle: $^{\#\#}p < 0.01$; post hoc test vs. Ctrl mice: $^{*}p < 0.05$, $^{**}p < 0.01$) and in hM4di mice (n = 9; red; right panels) (permutation-based mixed-design ANOVA: CNO doses $p < 0.001$; Ctrl/hM4di, $p = 0.13$; interaction, $p < 0.05$; post hoc test vs. Vehicle: $^{\#\#}p < 0.01$, $^{\#\#\#}p < 0.001$; post hoc test vs. Ctrl mice: $^{*}p < 0.05$) compared with respective Ctrl mice (n = 10; blue). **(C)** Comparison of cumulative distribution of SWS episode durations following Vehicle administration (dashed lines) and CNO treatments (solid lines; left panel: 1 mg/kg, right panel: 5 mg/kg) in hM3dq (n = 10; green), hM4di (n = 9; red), and Ctrl (n = 10; blue) mice. (A) and (B) Individual data for each mouse are displayed (lines; light colors) and averaged data are represented as mean ± SEM (bars). (C) Data are represented as mean (lines) ± SEM (light colors). See also Supplementary Figure S3.

Finally, we computed EEG power spectrums during SWS in response to CNO injections in Ctrl, hM3dq, and hM4di mice (Figure 5 and Supplementary Figure S3). Notwithstanding nonspecific effects within the δ frequency range in Ctrl mice (0.5–4 Hz; Figure 5A, D, and G), CNO treatments induced in hM3dq mice a significant decrease in spectral power within the 0.5–1.2 Hz frequency range (Figure 5B, E, H, and Supplementary Figure S3C), and in hM4di mice a significant and specific increase within the same frequencies (Figure 5C, F, H, and Supplementary Figure S3D). These observations might reflect a modulation in the density of slow oscillations that are thought to occur mainly during light SWS [27–29]. Additionally, spectral power was significantly increased in hM3dq mice within the 2–4 Hz range that might indicate increased slow waves (Figure 5I). These results likely indicate that MCH neurons, when active, could favor deep SWS [27–29]. In lines with this last observation, we found that CNO treatments in hM3dq mice significantly decreased the occurrence of spindle-like oscillations, that are mostly prevalent in periods of light SWS [30, 31], and the proportion of SWS time containing putative spindles (Figure 5J–L). The incidence of spindle-like oscillations was not affected in hM4di mice (Supplementary Figure S3, E and F).

Figure 5.

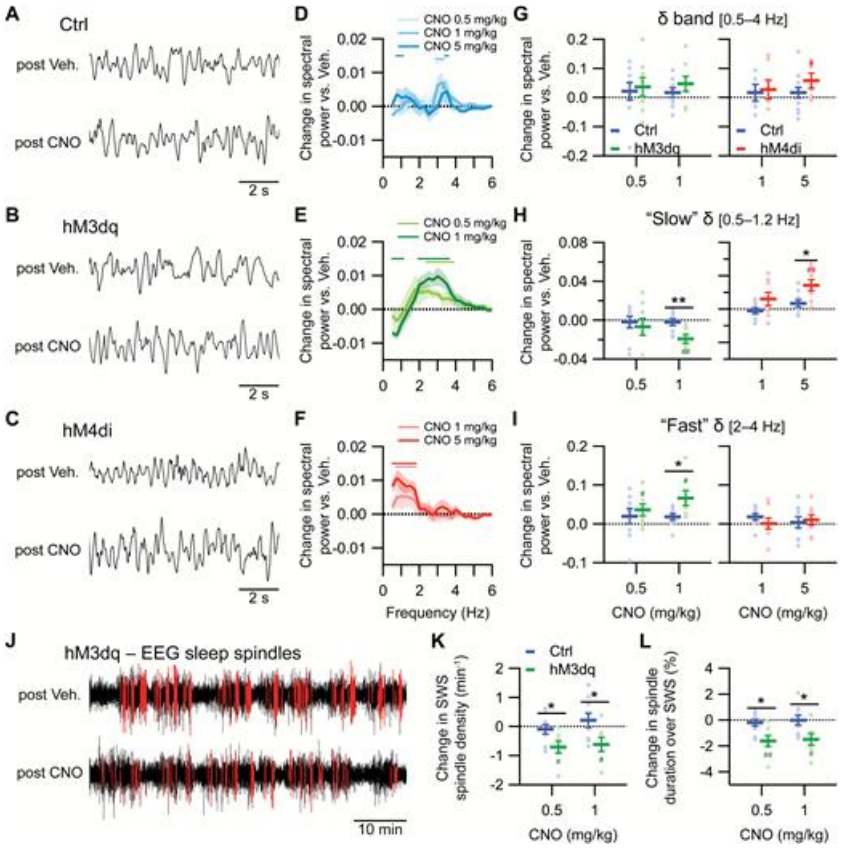

View large Download slide

EEG rhythmic activities during SWS are modulated by the MCH neurons. **(A–C)** Examples of frontal EEG signals recorded during SWS after CNO or Vehicle treatments in representative Ctrl (A), hM3dq (B), and hM4di (C) mice. **(D–F)** Changes in frontal EEG spectral power during SWS relative to Vehicle (dashed horizontal line) over the first 3 hr following CNO treatments in Ctrl (D; $n = 10$; blue), in hM3dq (E; $n = 8$; green), and hM4di (F; $n = 8$; red) mice (permutation-based two-way rmANOVA; for the three conditions, CNO doses, $p > 0.05$, frequency, $p < 0.001$, interaction, $p < 0.001$; post hoc test vs. Vehicle, horizontal bars above spectra indicate $p < 0.05$). Spectral data for individual doses of CNO are represented as mean (lines) ± SEM (light colors). **(G–I)** Changes in spectral densities induced by CNO treatments (relative to Vehicle) integrated over the entire δ band (0.5–4 Hz; G), the "slow" δ frequency range (0.5–1.2 Hz; H), and "fast" δ range (2–4 Hz; I) in hM3dq mice compared with Ctrl mice (left panels) (permutation-based mixed-design ANOVA: for the whole δ band: CNO doses, $p = 0.21$; Ctrl/hM3dq, $p = 0.71$; interaction, $p = 0.43$; for the "slow" δ band: CNO doses, $p < 0.05$; Ctrl/hM3dq, $p = 0.10$; interaction, $p < 0.01$; for the "fast" δ band: CNO doses, $p < 0.05$; Ctrl/hM3dq, $p = 0.24$; interaction, $p < 0.05$) and in hM4di mice compared with Ctrl animals (right panels) (permutation-based mixed-design ANOVA: for the whole δ band: CNO doses, $p < 0.01$; Ctrl/hM3dq, $p = 0.36$; interaction, $p = 0.27$; for the "slow" δ band: CNO doses, $p = 0.08$; Ctrl/hM3dq, $p < 0.01$; interaction, $p < 0.05$; for the "fast" δ band: CNO doses, $p = 0.65$; Ctrl/hM3dq, $p = 0.48$; interaction, $p = 0.87$). Individual data for each mouse are displayed (dots; light colors) and averaged data are represented as mean ± SEM (bars). **(J)** Representative example illustrating spindle-like oscillations detection (events in red) from frontal EEG recordings in one hM3dq mouse following Vehicle and CNO treatments. **(K–L)** Effect of CNO administration (relative to Vehicle) on the density of spindles during SWS episodes (K) and on the proportion of time in SWS occupied by spindles (L) in hM3dq mice ($n = 8$; green) compared with Ctrl mice ($n = 9$; blue) (permutation-based mixed-design ANOVA: for spindle density: CNO doses, $p < 0.05$; Ctrl/hM3dq, $p = 0.13$; interaction, $p < 0.05$; for spindle proportion: CNO doses, $p = 0.06$; Ctrl/hM3dq, $p = 0.09$; interaction, $p < 0.05$; post hoc test vs. Vehicle: $^{\#}p < 0.05$; $^{\#\#}p < 0.01$; post hoc test vs. Ctrl mice: $^{*}p < 0.05$). Individual data for each mouse are displayed (dots; light colors) and averaged data are represented as mean ± SEM (bars). See also Supplementary Figure S3.

Taken together, our chemogenetic results reveal that MCH neurons actively participate, during SWS, in the control of EEG oscillatory activities by accelerating EEG rhythms within the δ band that may promote deep sleep, and in the termination of SWS bouts. These mechanisms might ultimately result in PS release and in its consolidation.

Discussion

In the present study, we used chemogenetic tools to evaluate the effects on sleep of the bidirectional modulation of MCH neuron activity. In line with the recent paper by Gomez and collaborators [26] raising concerns about the specificity and biologically inert nature of CNO, we found that, when i.p.

administered to control mice that do not express hM3dq or hM4di receptors, this compound induced dose-dependent effects on sleep, statistically significant for doses higher than 5 mg/kg. These effects are probably caused by CNO reduction into clozapine, an atypical antipsychotic with potent effects on sleep probably through nonselective binding to dopaminergic, histaminergic, serotonergic, and adrenergic receptors [24, 25]. In addition, CNO inhibits the specific binding toward multiple endogenous receptors including histamine H1, serotonergic 5-HT_{2A}, muscarinic M1, M3, and M4, and dopamine D1 and D2 [26]. The latter could also contribute to the effects of CNO we observed in control animals. Thus, results obtained from CNO injections may be cofounded by CNO agonistic effects and clozapine converted from CNO. As a consequence, CNO-activated chemogenetic tools must be used with caution and experiments properly controlled at least in sleep research. This is especially the case when using inhibitory hM4di receptors, as they require large CNO doses to be activated and physiologically efficient.

Although MCH-expressing neurons are thought to participate in the regulation of sleep, in particular PS [5, 10–13, 17, 32], discrepant results have been reported concerning their actual role in or during SWS, mainly due to disparate technical or experimental procedures. Indeed, the chronic optical stimulation of ChR2-expressing MCH neurons during 24 hr increased SWS amounts only during the dark phase [12]. Their acute stimulation at the onset of a SWS episode did not change the duration of the ongoing episode [11]. In contrast, SWS amounts are decreased upon continuous stimulation for 3 hr during the light period [13]. In line with the latter study, we found here that CNO-mediated activation of MCH neurons during the light phase decreased SWS amounts by shortening episode duration, whereas their chemogenetic inhibition produced the opposite effect. This bidirectional effect suggests that MCH neurons might control the termination of SWS bouts even under basal conditions. We also observed complex and original effects on EEG rhythms during SWS after the chemogenetic activation of MCH neurons, showing simultaneously an increase in putative slow-waves (2–4 Hz), a decreased density of slow oscillations (<1Hz), and a dampening of spindle-like oscillations during SWS. These observations suggest that MCH neurons participate in the control of oscillatory activities during SWS likely through their direct neocortical and thalamic ascending projections [1]. Such a mechanism leading to an acceleration of cortical rhythms within the δ band might eventually participate in increasing SWS depth by enriching SWS with slow waves at the expense of light SWS dominated by slow oscillations and spindles [33–36].

These observations seem opposed to those harvested following cell-specific ablation of MCH neurons [13, 17]. These later studies reported a decrease of both SWS quantities and duration of SWS episodes, whereas we found that acute chemogenetic inhibition of MCH neurons increases SWS amounts and the length of SWS bouts. These discrepancies might reflect differences between acute and chronic manipulations of a given neuronal system. In few cases, both experimental strategies can produce similar outcomes such as the acute and chronic loss-of-function of NPY/AgRP neurons in the arcuate nucleus that both produce decreases in food intake [37, 38]. However, these experimental strategies can also produce different results. For instance, a chronic deletion of arcuate nucleus POMC neurons increases food intake [39], whereas their acute inhibition using chemogenetics does not significantly affect this function [40, 41]. Acute and chronic loss-of-function experiments can even produce completely opposite results: acute inhibition of somatostatin-expressing interneurons in the frontal cortex increases anxiety-like behaviors, whereas chronic inhibition or lesion of the same neurons produces the exact opposite effect [42]. In the latter situation, a chronic, long-lasting loss of function can lead to compensatory mechanisms and physiological adaptations that would not be triggered by an acute, short-lasting inhibition. Concerning MCH neurons, discrepancies between acute inhibition and lesion indicate their complex and time-dependent integration to sleep-regulatory networks. Moreover, in an attempt to reconcile these different studies, the effect on SWS of the ablation of MCH neurons can be interpreted as an enhanced SWS fragmentation with increased SWS to wake alternations, thus suggesting a defect in SWS consolidation [13, 17]. On the other hand, the acute chemogenetic inhibition of MCH neurons seems to produce a similar output by favoring long episodes of light SWS, whereas chemogenetic activation of MCH neurons facilitates deep SWS. Together, these results support a contribution of MCH neurons to the emergence of deeper and more consolidated SWS episodes.

We also observed that the chemogenetic activation of MCH neurons facilitates PS promotion and maintenance, in agreement with previous studies [5, 11–13, 15]. However, a puzzling result here is that we failed to detect any drastic change in PS after the chemogenetic inhibition of MCH neurons. In our experimental paradigm, the nonspecific effects of CNO alone might mask a decrease in PS amounts or the transfection rate of hM4di receptors in our animals could be insufficient to produce such an effect. However, similar negative results have been reported after optogenetic inhibition or cell-specific ablation of MCH neurons, whereas a suppression of PS would be predicted [11, 13, 15, 17]. Without questioning the fact that MCH neurons fire maximally during PS [10] and that activating MCH neurons facilitates PS onset and maintenance [11–15], the weak effects on PS of MCH neurons inhibition might raise the point of their actual involvement in PS control under basal conditions. Finally, a previously unreported modulation of the PS-specific EEG θ rhythm (increased peak frequency and power within the θ band) was observed following the chemogenetic activation of MCH neurons. This could occur likely through their synaptic projections to the hippocampus, the supramammillary nucleus, the medial septum, and cortical areas [1] in order to contribute to functions engaging these brain structures including during PS as learning, memory, or mood regulation.

Based on our present data, we propose a novel hypothesis regarding the functional role of MCH neurons in sleep that we trust encompass and reconcile apparent discrepancies in previous studies. When physiologically engaged during SWS, MCH neurons would trigger a cascade of events

successively aimed at deepening SWS, abbreviating the ongoing SWS episode, enhancing the probability of SWS to PS transition, and eventually consolidating the PS episode just initiated. In brief, MCH neurons would be crucially and actively involved in basic mechanisms occurring during SWS to pave the way to PS onset. Our proposal supposes a downstream regulation by MCH neurons not only on brainstem networks responsible for PS, as hypothesized previously [16, 18], but also by those controlling the ultradian rhythm of SWS [2, 4, 21, 43] where MCH neurons send efferent projection [1]. Further experiments are needed to elucidate the potential downstream targets mediating the SWS regulation by MCH neurons.

Supplementary Material

Supplementary material is available at *SLEEP* online.

Funding

This work was supported by CNRS UMR5292, INSERM U1028, and Université Claude Bernard Lyon I. C.V. received a 3 years PhD grants from *Ministère de l'Enseignement Supérieur, de la Recherche et de l'Innovation* (MESRI), and a 1 year post-doctoral grant from the French *Agence Nationale de la Recherche* (ANR, OPTOREM project).

Author Contributions

C.V., P.H.L., and P.F. designed experiments. C.V. collected and analyzed anatomical, in vitro electrophysiological, and polysomnographic data. All of the authors discussed the results. C.V. and P.F. wrote the manuscript.

Acknowledgments

We would like to thank Yoan Cherasse and Michael Lazarus (International Institute for Integrative Sleep Medicine, Tsukuba, Japan) for designing and providing AAVs used.

References

1. Bittencourt JCet al. The melanin-concentrating hormone system of the rat brain: an immuno- and hybridization histochemical characterization. *J Comp Neurol* . 1992;319(2):218–245.
Google Scholar Crossref PubMed

2. Fort Pet al. Alternating vigilance states: new insights regarding neuronal networks and mechanisms. *Eur J Neurosci* . 2009;29(9):1741–1753.
Google Scholar Crossref PubMed

3. Peyron Cet al. Role of the melanin-concentrating hormone neuropeptide in sleep regulation. *Peptides* . 2009;30(11):2052–2059.
Google Scholar Crossref PubMed

4. Saper CBet al. Sleep state switching. *Neuron* . 2010;68(6):1023–1042.
Google Scholar Crossref PubMed

5. Verret Let al. A role of melanin-concentrating hormone producing neurons in the central regulation of paradoxical sleep. *BMC Neurosci* . 2003;4:19.
Google Scholar Crossref PubMed

6. Sapin Eet al. A very large number of GABAergic neurons are activated in the tuberal hypothalamus during paradoxical (REM) sleep hypersomnia. *PLoS One* . 2010;5(7):e11766.
Google Scholar Crossref PubMed

7. Vas Set al. Nesfatin-1/NUCB2 as a potential new element of sleep regulation in rats. *PLoS One* . 2013;8(4):e59809.
Google Scholar Crossref PubMed

8. Jego Set al. Tuberal hypothalamic neurons secreting the satiety molecule Nesfatin-1 are critically involved in paradoxical (REM) sleep homeostasis. *PLoS One* . 2012;7(12):e52525.
Google Scholar Crossref PubMed

9. Arthaud Set al. Paradoxical (REM) sleep deprivation in mice using the small-platforms-over-water method: polysomnographic analyses and melanin-concentrating hormone and hypocretin/orexin neuronal activation before, during and after deprivation. *J Sleep Res* . 2015;24(3):309–319.
Google Scholar Crossref PubMed

10. Hassani OKet al. Melanin-concentrating hormone neurons discharge in a reciprocal manner to orexin neurons across the sleep-wake cycle. *Proc Natl Acad Sci USA* . 2009;106(7):2418–2422.
Google Scholar Crossref PubMed

11. Jego Set al. Optogenetic identification of a rapid eye movement sleep modulatory circuit in the hypothalamus. *Nat Neurosci* . 2013;16(11):1637–1643.
Google Scholar Crossref PubMed

12. Konadhode RRet al. Optogenetic stimulation of MCH neurons increases sleep. *J Neurosci* . 2013;33(25):10257–10263.
Google Scholar Crossref PubMed

13. Tsunematsu Tet al. Optogenetic manipulation of activity and temporally controlled cell-specific ablation reveal a role for MCH neurons in sleep/wake regulation. *J Neurosci* . 2014;34(20):6896–6909.
Google Scholar Crossref PubMed

14. Blanco-Centurion Cet al. Optogenetic activation of melanin-concentrating hormone neurons increases non-rapid eye movement and rapid eye movement sleep during the night in rats. *Eur J Neurosci* . 2016;44(10):2846–2857.
Google Scholar Crossref PubMed

15. Vetrivelan Ret al. Melanin-concentrating hormone neurons specifically promote rapid eye movement sleep in mice. *Neuroscience* . 2016;336:102–113.
Google Scholar Crossref PubMed

16. Luppi PHet al. Paradoxical (REM) sleep genesis by the brainstem is under hypothalamic control. *Curr Opin Neurobiol* . 2013;23(5):786–792.
Google Scholar Crossref PubMed

17. Varin Cet al. Sleep architecture and homeostasis in mice with partial ablation of melanin-concentrating hormone neurons. *Behav Brain Res* . 2015;298(Pt B):100–110.
Google Scholar PubMed

18. Szymusiak RS. New insights into melanin concentrating hormone and sleep: a critical topics forum. *Sleep* . 2013;36:1765–1766.

Google Scholar Crossref

19. Alexander GMet al. Remote control of neuronal activity in transgenic mice expressing evolved G protein-coupled receptors. *Neuron* . 2009;63(1):27–39.
Google Scholar Crossref PubMed

20. Armbruster BNet al. Evolving the lock to fit the key to create a family of G protein-coupled receptors potently activated by an inert ligand. *Proc Natl Acad Sci U S A* . 2007;104(12):5163–5168.
Google Scholar Crossref PubMed

21. Lazarus Met al. Arousal effect of caffeine depends on adenosine A2A receptors in the shell of the nucleus accumbens. *J Neurosci* . 2011;31(27):10067–10075.
Google Scholar Crossref PubMed

22. Kim Aet al. Optogenetically induced sleep spindle rhythms alter sleep architectures in mice. *Proc Natl Acad Sci USA* . 2012;109(50):20673–20678.
Google Scholar Crossref PubMed

23. Vyazovskiy VVet al. The dynamics of spindles and EEG slow-wave activity in NREM sleep in mice. *Arch Ital Biol* . 2004;142(4):511–523.
Google Scholar PubMed

24. Löffler Set al. Comment on “Impaired respiratory and body temperature control upon acute serotonergic neuron inhibition”. *Science* . 2012;337(6095):646; author reply 646.
Google Scholar Crossref PubMed

25. Hinze-Selch Det al. Effects of clozapine on sleep: a longitudinal study. *Biol Psychiatry* . 1997;42(4):260–266.
Google Scholar Crossref PubMed

26. Gomez JLet al. Chemogenetics revealed: DREADD occupancy and activation via converted clozapine. *Science* . 2017;357(6350):503–507.
Google Scholar Crossref PubMed

27. Crunelli Vet al. The slow (<1 Hz) rhythm of non-REM sleep: a dialogue between three cardinal oscillators. *Nat Neurosci* . 2010;13(1):9–17.
Google Scholar Crossref PubMed

28. Steriade Met al. Slow sleep oscillation, rhythmic K-complexes, and their paroxysmal developments. *J Sleep Res* . 1998;7(Suppl 1):30–35.
Google Scholar Crossref PubMed

29. Timofeev Iet al. Thalamocortical oscillations: local control of EEG slow waves. *Curr Top Med Chem* . 2011;11(19):2457–2471.
Google Scholar Crossref PubMed

30. Nuñez Aet al. Intracellular evidence for incompatibility between spindle and delta oscillations in thalamocortical neurons of cat. *Neuroscience* . 1992;48(1):75–85.
Google Scholar Crossref PubMed

31. Steriade Met al. Thalamocortical oscillations in the sleeping and aroused brain. *Science* . 1993;262(5134):679–685.

Google Scholar Crossref PubMed

32. Ahnaou Aet al. Blocking melanin-concentrating hormone MCH1 receptor affects rat sleep-wake architecture. *Eur J Pharmacol* . 2008;579(1-3):177–188.
Google Scholar Crossref PubMed

33. Nir Yet al. Regional slow waves and spindles in human sleep. *Neuron* . 2011;70(1):153–169.
Google Scholar Crossref PubMed

34. Achermann Pet al. Low-frequency (< 1 Hz) oscillations in the human sleep electroencephalogram. *Neuroscience* . 1997;81(1):213–222.
Google Scholar Crossref PubMed

35. Crunelli Vet al. Thalamic T-type Ca2+ channels and NREM sleep. *Cell Calcium* . 2006;40(2):175–190.
Google Scholar Crossref PubMed

36. Vyazovskiy VVet al. Sleep homeostasis and cortical synchronization: II. a local field potential study of sleep slow waves in the rat. *Sleep* . 2007;30(12):1631–1642.
Google Scholar Crossref PubMed

37. Luquet Set al. NPY/AgRP neurons are essential for feeding in adult mice but can be ablated in neonates. *Science* . 2005;310(5748):683–685.
Google Scholar Crossref PubMed

38. Krashes MJet al. Rapid, reversible activation of AgRP neurons drives feeding behavior in mice. *J Clin Invest* . 2011;121(4):1424–1428.
Google Scholar Crossref PubMed

39. Zhan Cet al. Acute and long-term suppression of feeding behavior by POMC neurons in the brainstem and hypothalamus, respectively. *J Neurosci* . 2013;33(8):3624–3632.
Google Scholar Crossref PubMed

40. Atasoy Det al. Deconstruction of a neural circuit for hunger. *Nature* . 2012;488(7410):172–177.
Google Scholar Crossref PubMed

41. Koch Met al. Hypothalamic POMC neurons promote cannabinoid-induced feeding. *Nature* . 2015;519(7541):45–50.
Google Scholar Crossref PubMed

42. Soumier Aet al. Opposing effects of acute versus chronic blockade of frontal cortex somatostatin-positive inhibitory neurons on behavioral emotionality in mice. *Neuropsychopharmacology* . 2014;39(9):2252–2262.
Google Scholar Crossref PubMed

43. Gallopin Tet al. Identification of sleep-promoting neurons in vitro. *Nature* . 2000;404(6781):992–995.
Google Scholar Crossref PubMed

Topic:

electroencephalography

hormones

hypothalamus

melanins

neurons

rem sleep

mice

sleep

sleep, slow-wave

chronic nonbacterial osteomyelitis

rhythm

Issue Section: Basic Science of Sleep and Circadian Rhythms

- Supplementary data

Supplementary data

Supplementary Figure - pdf file

View Metrics

Email alerts

New issue alert

Advance article alerts

Article activity alert

Subject alert

Receive exclusive offers and updates from Oxford Academic

More on this topic

What Does the Sleeping Brain Say? Syntax

and Semantics of Sleep Talking in Healthy Subjects and in Parasomnia Patients

Low Activity Microstates During Sleep

Temporal Characteristics of Delta Activity During NREM Sleep in Depressed Outpatients and Healthy Adults: Group and Sex Effects

Control of Blood Pressure During Sleep in Lambs

Related articles in

Web of Science

Google Scholar

Related articles in PubMed

Arousal and sleep circuits.

Direct GÎ±q Gating Is the Sole Mechanism for TRPM8 Inhibition Caused by Bradykinin Receptor Activation.

Mitochondrial dynamics and transport in Alzheimer's disease.

Magnetic Cell Sorting for In Vivo and In Vitro Astrocyte, Neuron, and Microglia Analysis.

Citing articles via

Web of Science (5)

Google Scholar

CrossRef

Latest | **Most Read** | **Most Cited**

Characterization of the sleep disorder of anti-IgLON5 disease

Actigraphic detection of periodic limb movements: development and validation of a potential device-independent algorithm. A proof of concept study

Simultaneous tonic and phasic REM sleep without atonia best predicts early phenoconversion to neurodegenerative disease in idiopathic REM sleep behavior disorder

Residual symptoms after natural remission of insomnia: associations with relapse over 4 years

Sleep duration and fragmentation in relation to

leukocyte DNA methylation in adolescents

Online ISSN 1550-9109
Print ISSN 0161-8105